American Mineralogist, Volume 101, pages 2689–2700, 2016

Growth of hydrothermal baddeleyite and zircon in different stages of skarnization

WEN WINSTON ZHAO[1], MEI-FU ZHOU[1,*], AND WEI TERRY CHEN[2]

[1]Department of Earth Sciences, The University of Hong Kong, Pokfulam Road, Hong Kong, China
[2]State Key Laboratory of Ore Deposit Geochemistry, Institute of Geochemistry, Chinese Academy of Sciences, Guiyang 550002, China

ABSTRACT

Both prograde and retrograde skarns from the Tengtie iron deposit, South China, contain rounded, euhedral, and anhedral zircon grains. Rounded grains were originally derived from detritus in carbonate rocks and were incorporated into the skarns. Euhedral and anhedral crystals are intergrown with various skarn minerals and are clearly hydrothermal in origin. These hydrothermal grains have low $(Sm/La)_N$ ratios and high La contents relative to typical magmatic ones and display flat LREE and subdued flattening of HREE chondrite-normalized patterns, similar to those of zircon crystallized from Zr-saturated fluids. Prograde skarns also contain baddeleyite rimed by zircon, which record a period of low Si activity during prograde skarnization relative to original magmatic-hydrothermal fluids. Hydrothermal zircon grains from Tengtie have variable Eu anomalies and slightly positive Ce anomalies, indicating that they may have crystallized from highly heterogeneous, but generally reducing fluids. They have low $\delta^{18}O$ values (–5.1 to –2.7 ‰), suggesting the involvement of meteoric fluids. Fluorine-rich fluids played an important role in remobilizing and transporting some high field strength elements (HFSE), including Zr, from the host granites into the skarn system. Reaction between HFSE-bearing fluids and carbonate rocks at the prograde stage decomposed F complexes to deposit HFSE-rich skarn minerals and baddeleyite. At the retrograde stage, alteration of the HFSE-rich skarn minerals released HFSE, including Zr and Sn, consequently producing a mineral assemblage of zircon, cassiterite, and retrograde skarn minerals. Dating results of zircons from the Tengtie skarn system by SIMS indicates roughly less than several million years duration for skarnization. Our study indicates that Zr was not only mobile locally under favorable conditions, but was also readily transported and deposited in different stages of skarnization.

Keywords: Baddeleyite, zircon, oxygen isotope, U-Pb geochronology, skarnization, HFSE

INTRODUCTION

Being one of the high field strength elements (HFSE), zirconium (Zr) has long been considered to be immobile during metamorphism or alteration (e.g., Ague 1994, 2003, 2011; Bebout et al. 1999; Breeding et al. 2004; Penniston-Dorland and Ferry 2008), and it is widely used for petrogenetic studies (e.g., Pearce and Cann 1973; Floyd and Winchester 1975; Drummond et al. 1996; Pearce 1996, 2008; Solar and Brown 2001; Ernst and Buchan 2003). However, an increasing body of evidence has shown that Zr can be mobilized by hydrothermal fluids and re-deposited as hydrothermal Zr-bearing minerals (e.g., Kerrich and King 1993; Nesbitt et al. 1999; Hoskin 2005; Pettke et al. 2005; Geisler et al. 2007; Lawrie et al. 2007; Pelleter et al. 2007; Kusiak et al. 2009; Toscano et al. 2014; Deng et al. 2015).

Skarns typically exhibit a temporal evolution with early-formed high-temperature phases precipitated from magmatic fluids overprinting isochemical thermal metamorphic marble and hornfels, in turn variably replaced by late low-temperature assemblages involved in meteoric and/or basinal fluids (Einaudi et al. 1981; Meinert et al. 2005; Rubenach 2013). Some studies have reported hydrothermal Zr-bearing minerals in contact zones between igneous rocks and carbonate sedimentary rocks (e.g., Gieré 1986; Rubin et al. 1989, 1993; Gieré and Williams 1992; Moine et al. 1998; Deng et al. 2015). Specifically, hydrothermal zircons in these skarns show various morphologies, and sometimes contain skarn mineral inclusions (e.g., Rubin et al. 1989; Deng et al. 2015). Furthermore, Rubin et al. (1993) proposed that leaching of igneous source rocks by F-rich hydrothermal fluids could be the major control on the precipitation of zircon in associated skarn assemblages. Recently, Deng et al. (2015) analyzed hydrothermal zircon by LA-ICP-MS showing a genetic relationship between iron skarn mineralization and the coeval magmatism. However, it remains unclear whether Zr-bearing minerals can form during different stages of skarnization, and what controls the growth of these minerals corresponding to the skarnization. Moreover, understanding the formation of Zr-bearing minerals in skarns can place significant constraints on the mechanism of mobilization, transportation, and deposition of Zr, and the fluid evolution of skarn systems, not only because of their presence, but also because they would be precisely dated using the U-Pb isotopic system to place tight temporal constraints on the timing of the ore-forming hydrothermal system if enough high precision of techniques were achieved.

Here, we report findings of hydrothermal baddeleyite and zircon in mineralized skarns from the Tengtie iron deposit,

*E-mail: mfzhou@hku.hk

0003-004X/16/0012–2689$05.00/DOI: http://dx.doi.org/10.2138/am-2016-5706

South China. Their textural relationships with other skarn minerals, and elemental and oxygen isotopic compositions indicate their formation in both the prograde and retrograde stages of skarnization. The results lead us to conclude that Zr was mobilized from granitic rocks by F-bearing hydrothermal fluids and that the formation of hydrothermal baddeleyite and zircon under different physical and chemical conditions protracted mineralization in the deposit. In addition, dating the magmatic zircon and skarn zircon provides important constraints on the duration of skarnization.

Geological setting and sampling

The present tectonic framework of South China was produced by multiple collisions of lithospheric blocks, and formed the South China Block, which is further divided by the northeast-southwest-trending Jiangshan-Shaoxing Suture (J-S Suture) into the Yangtze Block in the northwest and the Cathaysia Block in the southeast (Fig. 1a) (Zhao et al. 2011). The Yangtze Block is composed of Archean to Paleoproterozoic crystalline basement overlain by Neoproterozoic to Cenozoic sedimentary strata (Zhou et al. 2002; Yan et al. 2003). The Cathaysia Block is made up of Precambrian basement covered by the Neoproterozoic to Meosozoic sedimentary and volcanic sequences (Chen and Jahn 1998; Yu et al. 2005). The whole Cathaysia Block and the eastern part of the Yangtze Block witnessed an extensive Mesozoic igneous event, divided into the early (180–142 Ma) and late (140–66 Ma) phases, which were related to the subduction of paleo-Pacific plate (Zhou et al. 2006). Numerous deposits in the Nanling Range of the central part of South China are genetically related to this event (Hu and Zhou 2012; Mao et al. 2013).

The Tengtie iron skarn deposit in the southern Nanling Range occurs along the contact zone between the Devonian to Carboniferous strata and the Mesozoic granitic pluton (Fig. 1b). Devonian to Carboniferous strata are made up of dolomite and dolomitic limestone with sandstone and siltstone, and the carbonate layers are the main magnetite ore host. Early barren Sinian to Cambrian strata are composed of low-grade metamorphosed clastic rocks locally interbedded with carbonates (Zhao and Zhou 2015). The Mesozoic pluton is composed of early porphyritic (144.3 ± 0.8 Ma) and late fine-grained (106.4 ± 0.7 Ma) biotite granite as products of partial melting of the Mesoproterozoic continental crust under an extension tectonic setting (Gao et al. 2005). To the northwest, the Silurian pluton is granodiorite with an age of 419.1 ± 6.4 Ma, which was formed by partial melting of lower crust metasedimentary rocks with participation of mantle materials (Cheng et al. 2009). Ore bodies in this deposit are distributed in several mining districts, and aeromagnetic anomalies have been detected as areas for additional prospecting (Fig. 1b). The estimated ore reserves of the deposit include 72 Mt iron and 0.6 Mt non-ferrous metals (e.g., W, Mo, and Au), which together constitute one of the important Fe skarn deposits in South China (Zhao and Zhou 2015).

Massive and disseminated skarn ores are dominated by magnetite with variable amounts of chalcopyrite, pyrite, sphalerite, galena, and cassiterite. The paragenetic sequence shows early prograde and retrograde stages of silicate and oxide minerals, and a late sulfide stage of pyrite, shpalerite, galena, and chalcopyrite (Zhao and Zhou 2015). The prograde stage is characterized by diopsidic pyroxene, andraditic garnet, and humite, with accessary zircon, baddeleyite, fluorite, and apatite. The retrograde stage contains phlogopite, chlorite, epidote, quartz, and calcite, with minor amounts of zircon and cassiterite. The late retrograde stage is also accompanied by magnetite formation.

More than 100 samples of skarns and granites were collected from underground workings in the Tengtie (24°07′ N, 112°13′ E) and Dongyuan (24°08′ N, 112°20′ E) mining districts, as well as the fresh surface outcrop. Twenty samples were selected for zircon observation and separation. Early porphyritic biotite granite samples are TT14-13 from the underground working of the Tengtie mining district (~100 m away from the skarn contact), and LY14-35 (24°16′N, 112°08′E), LY14-45 (24°16′N, 112°08′E), LY14-54 (24°14′N, 112°08′E), and GD1228 (24°12′N, 112°09′E) from the fresh surface outcrop. They are composed of quartz (25–40 vol%), alkaline-feldspar (30–45 vol%), plagioclase

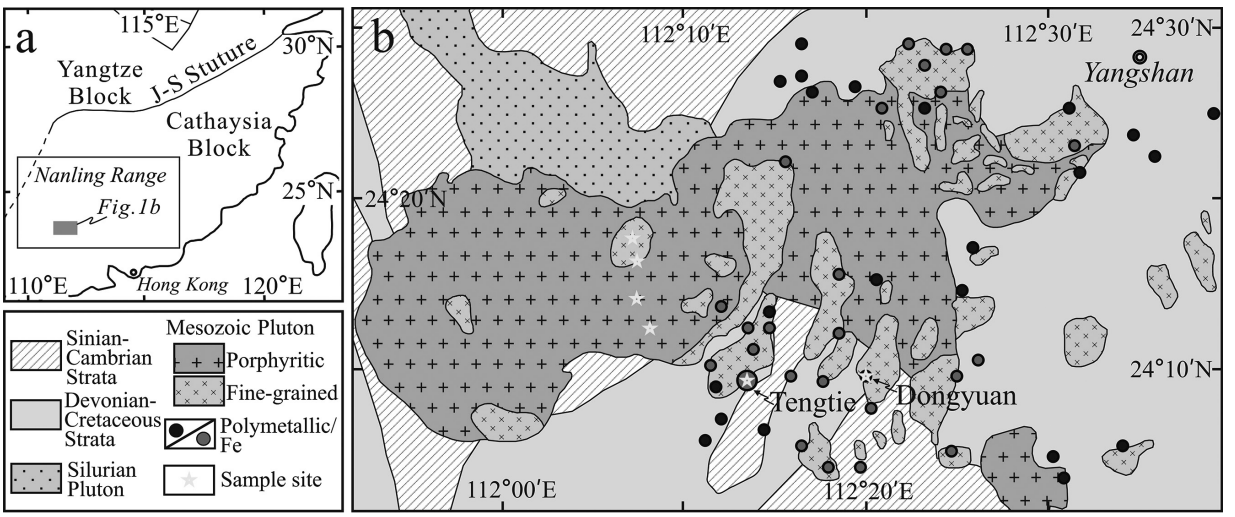

Figure 1. (**a**) Regional map of South China. (**b**) Location of the Tengtie skarn deposit and distribution of mining sites in the deposit (Zhao and Zhou 2015).

(15–25 vol%), and biotite (~5 vol%), with accessory zircon, magnetite, titanite, and apatite. Late fine-grained biotite granite samples are TT14-1617 and TT14-34 from the underground working of the Tengtie mining district (~90 m away from the skarn contact), and LY14-1617 (24°16′ N, 112°08′ E), LY14-34 (24°16′ N, 112°08′ E), and GD1227 (24°18′ N, 112°08′ E) from the fresh surface outcrop. They consist of quartz (30–35 vol%), alkaline-feldspar (35–45 vol%), plagioclase (20–30 vol%), and biotite (~5 vol%), with accessory minerals of zircon, apatite, titanite, and magnetite. Skarn samples are all exoskarn from the Tengtie (TT14-02, TT14-0203, TT14-04, TT14-05, TT14-117, F01, F02, F03, and F04) and Dongyuan (DY02) mining districts. They are composed of diopside (50–90 vol%), andratitic garnet (0–20 vol%), magnetite (0–30 vol%), epidote (0–20 vol%), chlorite (0–20 vol%), tremolite (0–10 vol%), and calcite (0–10 vol%), and quartz (0–5 vol%), with minor amounts of zircon, fluorite, and apatite.

Analytical techniques

Hand specimens were sawed into rock chips for preparation of mineral separates and thin sections, respectively. Zircons were separated from 10 granite samples (TT14-1617, TT14-34, TT14-13, LY14-1617, LY14-34, LY14-35, LY14-45, LY14-54, GD1227, and GD1228) and three skarn samples (TT14-05, TT14-117, and TT14-0203), using standard density and magnetic separation techniques. Zircon grains, together with zircon U-Pb and oxygen isotope standards (Qinghu, Penglai, and Plésovice), were cast in epoxy grain mounts, which was then polished to section the crystals in half for analysis. Uncoated thin sections and mounts were documented using transmitted and reflected light micrographs, and then scanning electron microscopy (SEM) at the Electron Microscope Unit, The University of Hong Kong (HKU). Selected sections and mounts were further vacuum-coated with high-purity gold and carbon, respectively, for Cathodoluminescence (CL) imaging at the Department of Earth Sciences, HKU, and electron microprobe (EMP) analyses at the State Key Laboratory of Continental Tectonics and Dynamics, Chinese Academy of Geological Sciences, Beijing. Gold-coated zircon mount samples (TT14-05, TT14-117, LY14-1617, LY14-34, LY14-35, LY14-45, and LY14-54) were then used for U-Th-Pb and oxygen isotopic analyses (Li et al. 2009, 2010; Tang et al. 2015) at the Institute of Geology and Geophysics, Chinese Academy of Sciences, Beijing. Re-polished sections (DY02, F02, TT14-04, and TT14-02) and mount samples (GD1227 and GD1228) were used for in situ trace element analyses by laser ablation ion coupled plasma mass spectrometry (LA-ICP-MS) for zircon (Liu et al. 2010) at the State Key Laboratory of Geological Processes and Mineral Resources, China University of Geosciences, Wuhan, and for clinopyroxene and garnet (He et al. 2015) at the Chinese Academy of Sciences Key Laboratory of Crust-Mantle Materials and Environments, University of Sciences and Technology of China, Hefei. Four fluid inclusion sections (F01, F02, F03, and F04) were made for microthermometry studies of calcite from the retrograde skarn stages at the Guangzhou Institute of Geochemistry, Chinese Academy of Sciences, Guangzhou. Details regarding the analytical techniques above are provided in the Supplementary Appendix[1].

Petrography of zircon

Four types of zircon (Type 1, Type 2, Type 3, and Type 4) were recognized based on their occurrences and morphologies (Figs. 2–3; Supplementary[1] Figures). Type 1 and Type 2 zircons, sampled from skarns in the Tengtie and Dongyuan districts, are all transparent. Type 1 zircon is further subdivided into Type 1a and Type 1b for prograde and retrograde skarn assemblages, respectively. Type 1a zircon from the prograde skarns is always as anhedral rims around anhedral baddeleyite with sharp contacts, and usually less than 15 μm in size (Figs. 2a–2b; Supplementary[1] Fig. S1). The baddeleyite and zircon, accompanied by apatite and fluorite, always occur in the pores of the prograde skarn minerals (e.g., diopside). Type 1b zircon from the retrograde skarns ranges in size from nanometers to more than 100 μm, but most are less than 30 μm across (Figs. 2c–2d; Supplementary[1] Fig. S2–S3). Large grains of Type 1b are euhedral or subhedral associated with cassiterite, calcite, epidote, and chlorite with curved or straight contacts. Some of these grains contain epidote or calcite inclusions. Tiny-size Type 1b is usually needle-like along the cleavages of the chlorite (Fig. 2e). Both the large and small Type 1b grains are associated with magnetite mineralization in the retrograde skarns (Fig. 2f). Under CL, a zonation pattern is seen in which individual zones appear to be wide and faint (Fig. 2g). Two-phase fluid inclusions, about 5 μm in diameter, occur in large, euhedral Type 1b zircon grains (Fig. 2h). Type 2 zircon from skarns is usually rounded, which is obviously different from Type 1 (Figs. 3a–3d; Supplementary[1] Fig. S4). They are about 30 μm in width, and often have a dark, faint zoning inner core with white homogeneous rims under CL. Typically, most grains of this type are free of inclusions.

Type 3 zircon from the late fine-grained biotite granite and Type 4 zircon from the early porphyritic biotite granite are transparent and translucent (Fig. 3; Supplementary[1] Fig. S4), respectively. Transparent Type 3 zircon grains are mostly euhedral with a size of around 200 μm and typical magmatic oscillatory zoning (Fig. 3f), and contain apatite inclusions (Fig. 3e). In contrast, translucent Type 4 zircon is usually larger than 200 μm, and shows complex textures under BSE and CL imaging, which generally consists of dark and bright domains with a sharp interface (Figs. 3i–3j). The BSE-dark domains typically contain pores and inclusions of HFSE-rich minerals (e.g., thorite), whereas the BSE-bright parts are mostly free of inclusions. Under CL images, the BSE-dark parts are black with no visible textures, whereas the BSE-bright parts have weak zoning with narrow bands. Fractured and porous textures are common in the translucent zircon grains (Fig. 3i).

Analytical results

Type 1 zircons from skarns and transparent Type 3 zircons from the late fine-grained granite have similar major element compositions, different from those of the translucent Type 4 zircons in the early porphyritic granite, which typically have distinctly lower ZrO_2 (48.8 to 56.8 wt%), slightly lower SiO_2 (29.2 to 32.5 wt%), and higher U (4.07 to 8.04 wt%) and Hf (1.42 to 3.03 wt%) (Table 1). The relatively low oxides totals (95.02 to 97.71 wt%) of the translucent zircons may be due to the incorporation of a hydrous component in the radiation-damaged structure (Nasdala et al. 2001) or the porous surface as mentioned earlier. Specifically, the BSE-bright domains of the translucent Type 4 zircons have relatively high Zr and low U concentrations compared to the BSE-dark domains of these grains, but the Si and Hf concentrations do not show apparent variations in a single grain under X-ray elemental mappings (Figs. 3m–3p).

In the skarns, the Type 1b zircons have $\delta^{18}O$ values (–5.1 to –2.7‰) much lower than the rounded Type 2 zircon grains (5.0 to 12.0‰). Transparent Type 3 zircon grains from the late fine-grained biotite granite have $\delta^{18}O$ values (5.8 to 7.7‰) similar to

[1]Deposit item AM-16-125706, Supplemental Figures, Tables, and Appendix. Deposit items are free to all readers and found on the MSA web site, via the specific issue's Table of Contents (go to http://www.minsocam.org/msa/ammin/toc/2016/Dec2016_data/Dec2016_data.html).

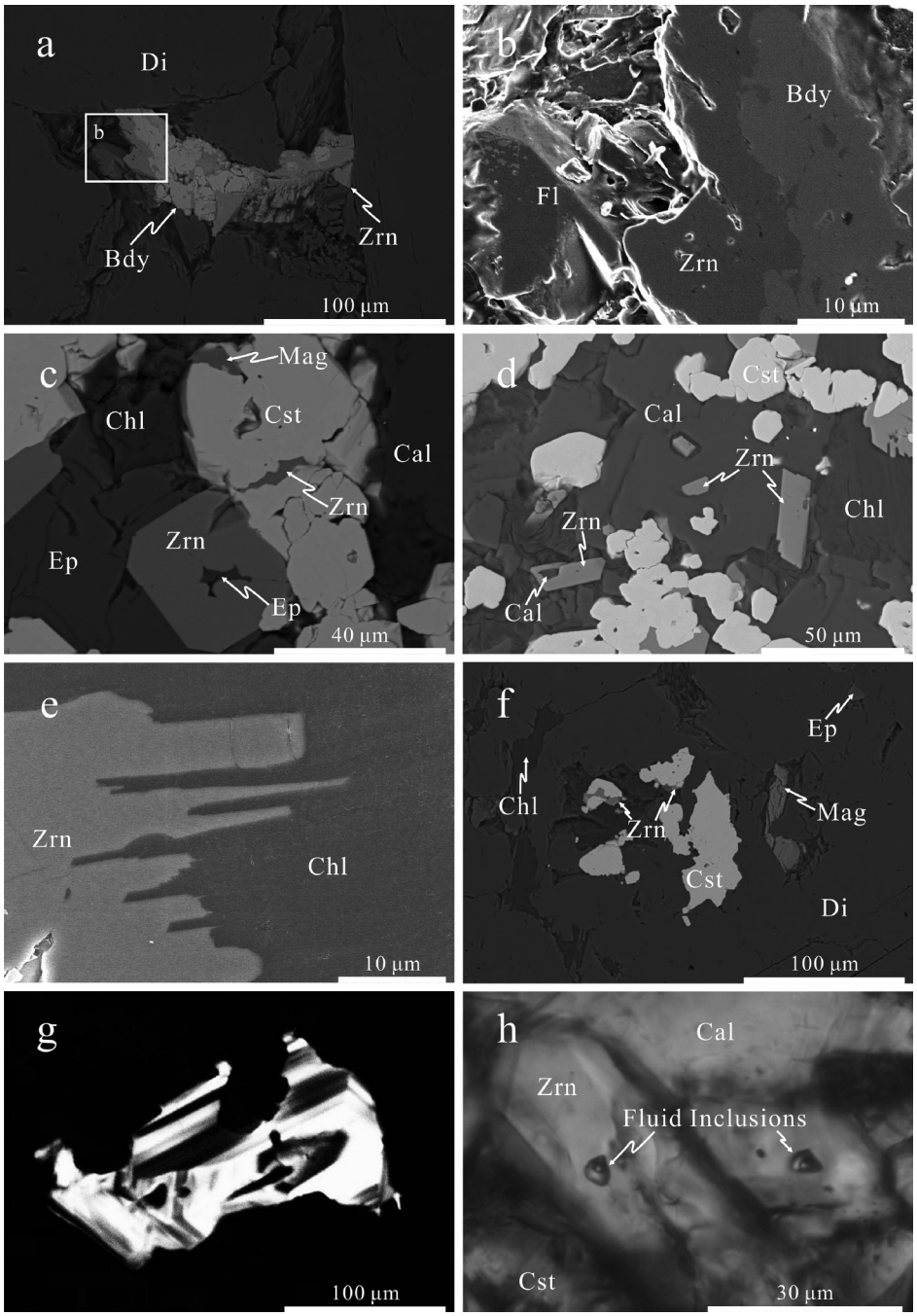

FIGURE 2. Microscopic images of hydrothermal Type 1 zircon in thin sections from the Tengtie skarn. (**a**–**f**) BSE images. (**g**) CL image. (**h**) Transmitted-light image. Mineral name abbreviations (Whitney and Evans 2010): baddeleyite = Bdy, calcite = Cal, cassiterite = Cst, chlorite = Chl, diopside = Di, epidote = Ep, fluorite = Fl, magnetite = Mag, zircon = Zrn.

those of typical magmatic zircon (e.g., Valley 2003). The $\delta^{18}O$ values of inclusion- and crack-free domains in the translucent Type 4 zircons from the early porphyritic biotite granite are roughly similar, ranging from 5.2 to 7.9 ‰ with a peak slightly lower than that of the transparent Type 3 zircon (Fig. 4 and Supplementary[1] Table S1). However, due to metamictization or possible later hydrothermal alteration, the $\delta^{18}O$ values of the translucent, high-U Type 4 zircons could not represent the primary signature. However, the narrow $\delta^{18}O$ ranges indicate that the different matrix effects would have less impact on the analyses, but the later potential homogeneous hydrothermal fluids might play a more important role (e.g., Wang et al. 2014).

The low-U content of zircon is more suitable for SIMS U-Pb dating than high-U zircons, because extremely high U

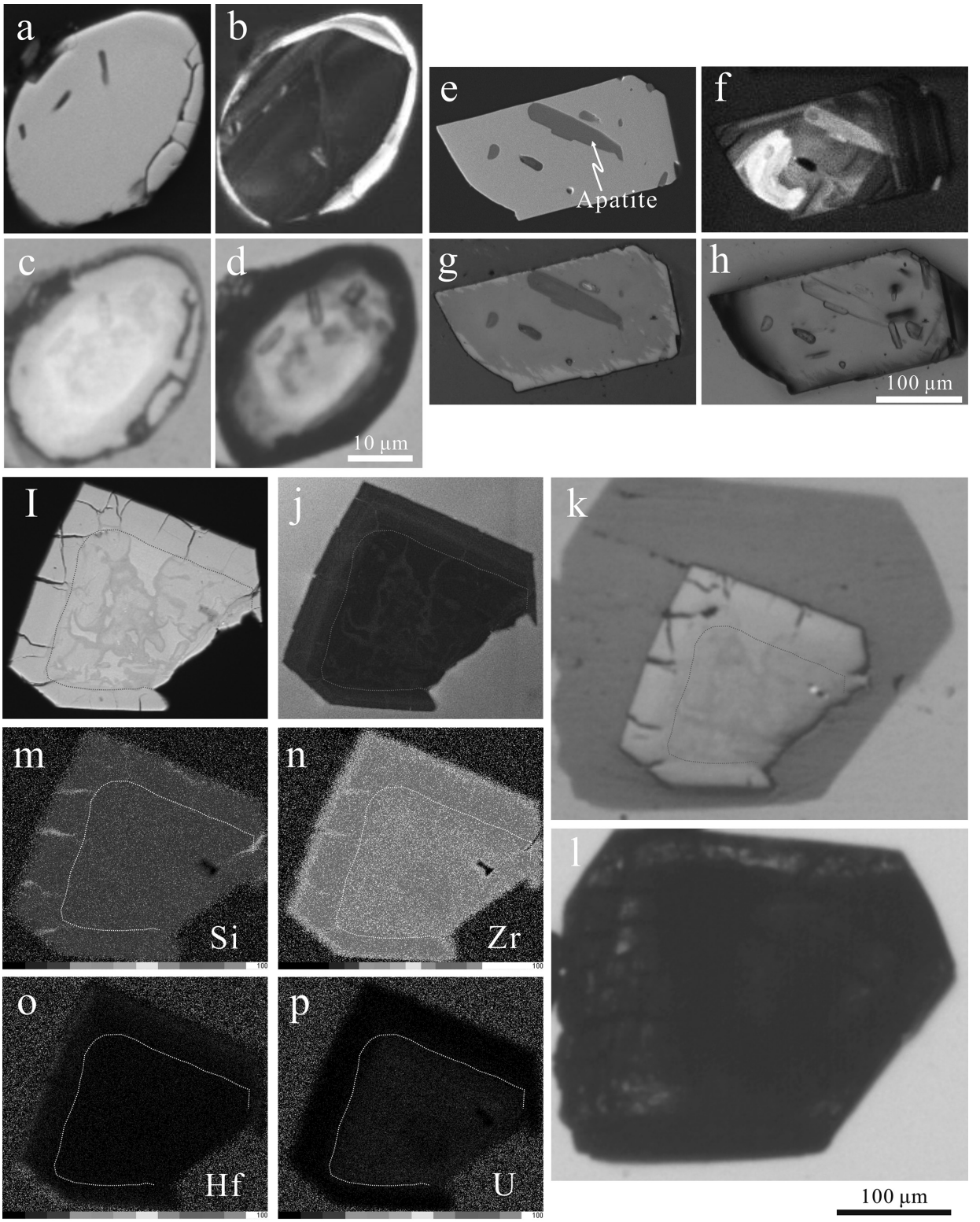

FIGURE 3. Microscopic images of the rounded Type 2 zircon separates (**a**–**d**). Transparent Type 3 zircon separates from the late granitic phase (**e**–**h**), and translucent Type 4 zircon separates from the early granitic phase (**i**–**p**) separates from Tengtie deposit. (**a**, **e**, **i**) BSE image. (**b**, **f**, **j**) CL image. (**c**, **g**, **k**) Reflected-light image. (**d**, **h**, **l**) Transmitted-light image (**m**, **n**, **o**). (**p**) EDS elemental mapping image.

Table 1. EMPA data (wt%) for zircon and baddeleyite

	SiO_2	CaO	P_2O_5	Y_2O_3	ZrO_2	La_2O_3	Ce_2O_3	Eu_2O_3	Sm_2O_3	Lu_2O_3	HfO_2	TiO_2	UO_2	Total
Type 1 zircon														
TT14-05-1	32.5	–	–	–	65.1	0.10	0.13	0.18	0.09	–	1.06	0.02	0.56	99.68
TT14-05-2	32.6	0.03	–	0.01	63.9	–	0.27	–	–	–	0.72	0.06	0.35	98.00
TT14-05-3	32.4	0.04	–	–	64.8	0.23	0.24	–	0.02	0.23	0.58	0.02	0.58	99.17
TT14-05-4	32.3	–	–	–	64.8	–	0.37	–	0.15	–	1.05	0.01	0.12	98.84
TT14-05-5	32.1	0.06	–	–	62.8	0.25	0.49	0.01	0.10	–	1.15	0.03	0.27	97.30
Type 3 zircon														
TT14-1617-1	32.4	0.17	0.30	0.26	63.6	0.13	0.02	–	–	0.12	1.24	0.03	0.09	98.36
TT14-1617-2	32.7	0.02	–	–	64.6	0.10	0.03	–	–	–	1.14	0.06	–	98.71
TT14-34-1	32.4	0.03	0.07	0.26	64.6	–	0.08	–	–	–	0.77	0.03	0.04	98.23
TT14-34-2	33.1	–	0.05	0.05	64.1	–	0.02	0.12	0.21	–	1.50	–	0.03	99.11
Type 4 zircon														
TT14-13-1	32.4	0.36	0.67	3.49	48.8	0.06	–	–	–	0.39	1.42	0.02	8.04	95.73
TT14-13-3	30.5	0.01	0.23	1.90	56.6	–	0.33	0.04	0.05	0.48	1.96	0.03	5.66	97.71
TT14-13-2	32.1	0.18	0.47	2.47	54.7	–	0.03	0.02	–	0.25	1.54	0.07	4.93	96.71
TT14-13-6	30.8	–	0.35	1.95	56.5	0.12	0.13	0.03	–	0.27	2.77	0.01	4.57	97.50
TT14-13-5	29.2	1.22	0.75	2.75	52.2	–	0.06	0.03	–	0.44	3.03	0.08	5.30	95.02
TT14-13-4	32.5	3.21	0.63	2.71	49.5	–	0.05	–	0.10	0.32	2.85	–	4.75	96.59
TT14-13-7	30.0	–	1.11	3.56	52.8	–	–	0.08	–	0.30	2.87	0.03	5.58	96.25
TT14-13-8	31.6	0.24	0.94	2.91	52.2	–	0.27	–	–	0.43	2.66	–	5.26	96.58
TT14-13-9	31.0	0.01	0.33	1.84	56.8	–	0.02	–	–	0.35	2.59	–	4.07	96.97
TT14-13-10	32.1	0.09	0.26	1.66	55.1	–	–	0.18	–	0.06	2.62	0.01	4.53	96.57
Baddeleyite														
TT14-04-BD2	–	–	–	–	97.2	0.15	–	–	0.04	0.15	0.48	0.05	–	98.07
TT14-04-BD3	–	–	–	–	98.7	0.11	–	–	–	0.12	1.44	0.01	–	100.42
TT14-04-BD4	–	–	–	–	98.6	–	–	–	0.12	–	1.39	–	–	100.10

Note: Dash (–) means below detection limit of 0.01 wt%.

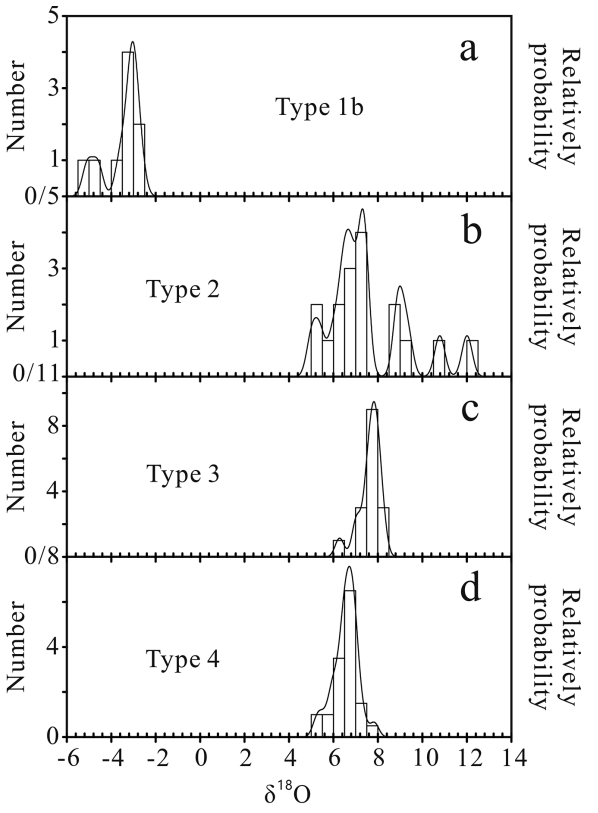

Figure 4. Oxygen isotope ranges of zircon from the Tengtie deposit.

may cause intense metamictization leading to matrix effects on SIMS analyses (White and Ireland 2012; Pidgeon et al. 2013; Wang et al. 2014). Analyses of Type 3 and Type 1b zircons yield concordia ages of 99.3 ± 0.5 Ma (N = 9; MSWD = 0.0004) and 97.5 ± 0.7 Ma (N = 5; MSWD = 5.2), respectively (Figs. 5a and 5c). However, the rounded zircons from the skarn have a wide range of ages with the youngest $^{206}Pb/^{238}U$ age at 416.2 ± 7.1 Ma, and some points plotting off concordia (Fig. 5b). Dating of high-U radiation damaged zircon provide dispersed unreal ages ($^{206}Pb/^{238}U$ ages from 88.7 ± 1.3 to 137.3 ± 2.1 Ma; Supplementary[1] Table S2) younger or older than the unknown real age (e.g., Wang et al. 2014).

The translucent Type 4 zircons have total concentrations of REE (7039–14259 ppm) much higher than the transparent Type 3 zircons (550–1758 ppm) and Type 1b zircons (58–143 ppm) (Supplementary[1] Table S3). The transparent zircons have more pronounced positive Ce anomalies (Ce/Ce* = 11–156) than the translucent (1–6) and irregular (3–15) grains (Fig. 6). The Type 1b zircons have variable Eu anomalies (Eu/Eu* = 0.16–1.48), whereas all the zircons from the granites have significantly negative Eu anomalies (Fig. 6).

Based on the core-rim texture in different mineral assemblages and major element variations (e.g., Einaudi et al. 1981; Meinert et al. 2005), diopside and andratitic garnet from early prograde and late prograde assemblages were distinguished and show distinct trace elemental compositions (Supplementary[1] Table S4). In the prograde skarn stages, the water/rock ratios were high, and thus the partitioning of trace elements in the prograde skarn minerals would be mainly buffered by the fluid compositions (Gaspar et al. 2008). The early prograde skarn minerals are enriched in HFSE with respect to the late prograde

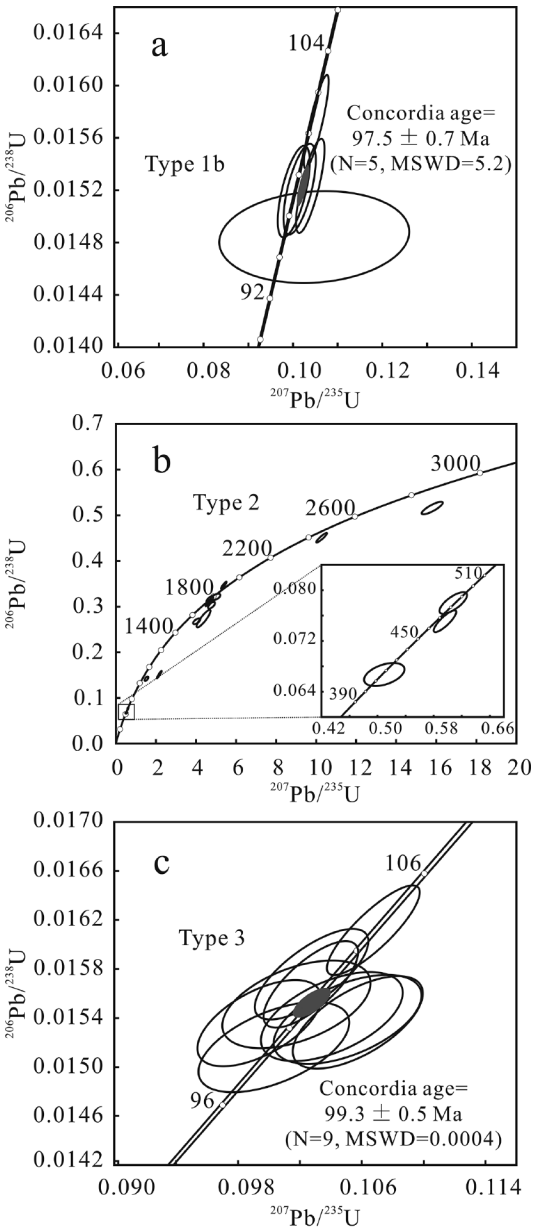

Figure 5. SIMS U–Pb concordia age plots for zircons from the Tengtie skarn deposit. (**a**) Hydrothermal Type 1b zircons from the retrograde stage of the Tengtie skarns. (**b**) Detrital Type 2 zircons from the Tengtie skarns. (**c**) Magmatic Type 3 zircons from the late granitic phase of the Mesozoic pluton.

skarn minerals (e.g., Ti, Zr, Nb, Sn, and REE) (Fig. 7). Also, it is remarkable that skarn minerals from both early and late prograde stages are typically enriched in light rare earth elements (LREE) relative to heavy rare earth elements (HREE).

Calcite grains in the retrograde skarns coexisting with the Type 1b zircon grains contain two-phase fluid inclusions, ranging from 5 to 15 μm, which are similar to those in hydrothermal zircon grains (Fig. 3h). Homogenization temperatures of these fluid inclusions in associated calcite range from ~330 to ~230 °C (Fig. 8). Salinity of these aqueous fluid inclusion, estimated using the data of Bodnar (1994) for the NaCl-H_2O system, ranges from 6.6 to 17.5 wt% NaCl equiv. (Supplementary[1] Table S5).

Discussion

Baddeleyite and zircon in skarn systems

Zircon grains from the Tengtie skarns have various morphologies and chemical compositions indicating different origins. The Type 2 zircon grains, with their well-rounded edges, are unlikely to have grown in situ in the skarn. Indeed, they have wide variations of oxygen isotope values (5.0 to 12.0‰) (Fig. 4b), consistent with their diverse origins. Considering that the host Devonian strata in the region are interpreted to have formed in a platform-basin system (Chen et al. 2001), which may have various terrestrial sources, the Type 2 grains are interpreted as detrital in origin. Such an interpretation is also supported by the wide range of their ages, which are concentrated between

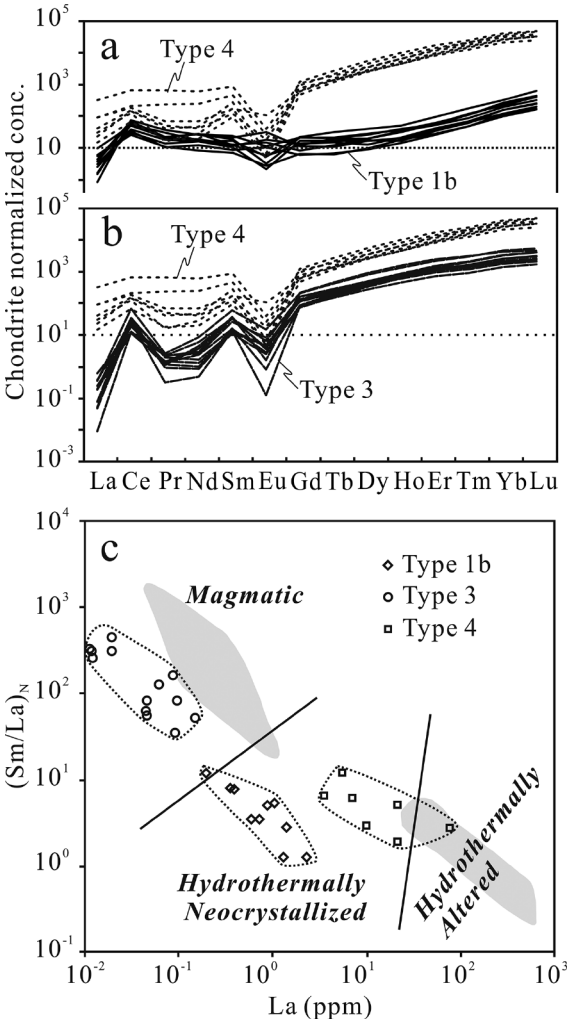

Figure 6. (**a** and **b**) Chondrite-normalized zircon REE patterns. (**c**) $(Sm/La)_N$ vs. La diagram. The shadowed field is defined by Hoskin (2005), and the dashed straight line by Kirkland et al. (2009). Chondrite normalizing values are from McDonough and Sun (1995).

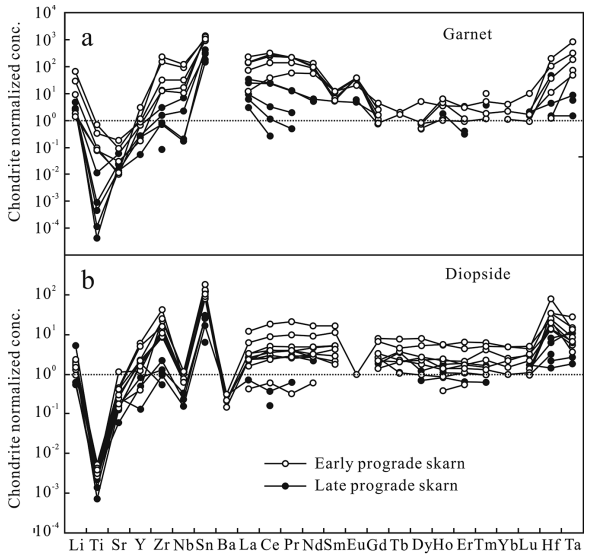

FIGURE 7. Spider diagrams of chondrite-normalized trace elements from skarn minerals from both early and late prograde stages. (**a**) Garnet. (**b**) Diopside. Chondrite normalizing values from McDonough and Sun (1995).

~1.7 to ~1.9 Ga with the youngest age of ~416 Ma (Fig. 5b). These age distributions indicate that the major contributor to the sedimentary detritus could be Paleoproterzoic sources in South China with minor contributions from Caledonian sources, such as the Silurian pluton in this region.

In contrast, the Type 1 zircon grains, including euhedral and anhedral ones, are unlikely to be detrital in origin, because their ages of ~98 Ma are much younger than those of the strata (Fig. 5a). The close association of the hydrothermal baddeleyite and zircon with different skarn minerals indicates that the zircon has grown during different stages of skarnization, and thus is hydrothermal in origin (e.g., Deng et al. 2015). Such an interpretation is further supported by the presence of two-phase fluid inclusions in the Type 1 zircon grains, a feature that is similar to hydrothermal zircons formed in some high-sulfidation Au–Ag–(Cu) deposits (Lawrie et al. 2007) and skarn Fe deposits in North China (Deng et al. 2015). In addition, Type 1 zircons have high-La contents and low-$(Sm/La)_N$ values relative to magmatic ones and display flat LREE and gently positively sloping HREE patterns (Fig. 6), typical of zircon precipitated from hydrothermal fluids (e.g., Hoskin 2005; Pelleter et al. 2007; Kirkland et al. 2009).

In the prograde skarns, anhedral baddeleyite, rimmed by Type 1a zircon, is present in interstitial pores of the prograde skarn minerals (e.g., diopside) (Fig. 2a). It is noted that such zircon-bearing pores do not contain any retrograde minerals, different from the pores that suffered from retrograde alteration. This feature thus indicates that the formation of both the baddeleyite and Type 1a zircon might slightly postdate the prograde skarn minerals, and should be products of prograde skarnization. The baddeleyite-zircon association is not common in skarns. The most plausible explanation is that during the skarnization, baddeleyite might crystallize first from relatively low Si-bearing fluids. Subsequent incursion of the SiO_2-rich hydrothermal fluids partially altered it to form zircon rims during successive periods of skarn alteration, in response to the increase of silica activity (e.g., Davidson and Van Breemen 1988). Such a phenomenon is also common in metamorphosed mafic dykes during the initial stages of metamorphism, where baddeleyite can decompose to a polycrystalline zircon via the reaction: $ZrO_2 + SiO_2 = ZrSiO_4$ (Davidson and Van Breemen 1988; Söderlund et al. 2008).

Similarly, in the retrograde skarns, hydrothermal Type 1b zircons are closely associated with the retrograde skarn minerals. Some of them contain inclusions of minerals identical to those from the retrograde skarns (Figs. 2c–2d), and some occur as intergrowth in the cleavages of chlorite (Fig. 2e). These features indicate that both the zircon and retrograde skarn minerals precipitated at the same time. Therefore, hydrothermal zircon must have formed during the retrograde stages of skarnization.

In general, Zr in hydrothermal fluids, which results in the formation of hydrothermal baddeleyite and zircon in skarns, can potentially be sourced by local remobilization of Zr or transported from external sources by fluids. A potential local source of Zr might be the detrital Type 2 zircons. However, no evidence of dissolution on the rounded Type 2 zircon surfaces was seen. Localized minor cracks in this type of zircon could have been created during mineral separating processes (Figs. 3a–3d; Supplementary[1] Fig. S4). In addition, the low U contents in Type 2 zircons would not allow for much radiation damage of the crystallographic lattice, which, if it occurred, would enhance dissolution and recrystallization (e.g., Geisler et al. 2001; Dempster et al. 2004). This would argue against the possibility of local remobilization of detrital zircon grains during much later hydrothermal events. Thus, the Zr in the fluids was likely derived from external sources. It is suggested that during skarnization, both early magmatic-hydrothermal and late meteoric-hydrothermal fluids can leach and transport components from external sources (Meinert et al. 2005). The occurrence of hydrothermal baddeleyite and zircon in the prograde skarns at Tengtie suggests that Zr was probably transported into the skarn system at the beginning of skarnization. Indeed, the high water/rock ratios, present during early prograde skarnization, imposed pronounced HFSE concentrations on diopside and garnet, especially Zr and Sn (Fig. 7), implying that the magmatic-hydrothermal fluids, which evolved from the granitic magmas, were already enriched in HFSE (e.g., Smith et al. 2004; Gaspar et al. 2008; Ismail et al. 2014).

Alternatively, modification of zircon is well recorded in the radiation-damaged domains of the translucent zircons from the early phase of the Mesozoic pluton (Figs. 3i–3l). Such a feature is similar to the experimental results of Geisler et al. (2007). Hence, it seems that Zr could be sourced from such mobilization processes. However, this possibility is excluded by the general acceptance that alteration of high-U zircon usually occurs after the crystal structure is damaged by radiation, which takes at least several millions of years under low temperature (e.g., Mezger and Krogstad 1997; Geisler et al. 2003). Also, it has been demonstrated in several studies (e.g., Mursic et al. 1992; McLaren et al. 1994; Mezger and Krogstad 1997; Rizvanova et al. 2000) that metamict zircon can recover their crystallinity rapidly under the laboratory condition above about 600 °C. During the latter stages of granitic crystallization, magmatic-hydrothermal fluids evolved from residual melts would generally be around 650 °C

(Einaudi et al. 1981; Meinert et al. 2005). As such, it is possible that the initially radiation damaged high U, Type 4 zircon in the Mesozoic pluton had already recrystallized when the late granitic phase was intruding. This is further supported by the fact that the early high U, Type 4 cores are present in the late Type 3 zircons from the late granitic phase (Supplementary[1] Fig. S4). The Type 3 zircons have a SIMS age of 99.3 ± 0.5 Ma, comparable to that of the hydrothermal Type 1b zircon (97.5 ± 0.7 Ma). Therefore, the annealing and leaching processes experienced by the high-U, Type 4 zircon might not correspond to the main, high-temperature skarnization event. Overall, the Zr source for the hydrothermal baddeleyite and zircon, during different stages of skarnization, most likely was from the late intrusive phase of the Mesozoic granitic pluton.

Nature of hydrothermal fluids

The association of the hydrothermal zircon with fluorite in the skarns implies that F-rich fluids were most likely responsible for the mobilization and transportation of Zr as $ZrF_n(OH)_m^0$ (cf. Salvi and Williams-Jones 1996; Salvi et al. 2000; Migdisov et al. 2011). It is generally accepted that REEs can form stable highly mobile, complexes with both fluoride and chloride anions (e.g., Haas et al. 1995; Migdisov and Williams-Jones 2007; Migdisov et al. 2009; Tropper et al. 2011; Tropper et al. 2013). However, while REE chlorides are relatively soluble at moderate temperatures (~300 to ~500 °C), REE fluorides are relatively insoluble at these temperatures, which limits the amount of REEs transported as REE fluoride complexes (Williams-Jones et al. 2012; Williams-Jones and Migdisov 2014). As such, the hydrothermal Type 1b zircons deposited from such F-rich fluids have the lowest REE contents compared to the other zircon grain types (Fig. 6). Notably, the different degrees of enrichment of LREE in the prograde diopside and andraditic garnet (Fig. 7) is in agreement with the relatively high mobility of LREE in F-rich fluids compared to HREE (excluding Y, which here is strongly partitioned into garnet) (e.g., Migdisov et al. 2009; Williams-Jones et al. 2012; Linnen et al. 2014; Williams-Jones and Migdisov 2014). Hence, we propose that the F-rich, magmatic-hydrothermal fluids were evolved from the late granitic magmas, with the REE (LREE > HREE) and HFSE, interacting with the carbonates to form skarns.

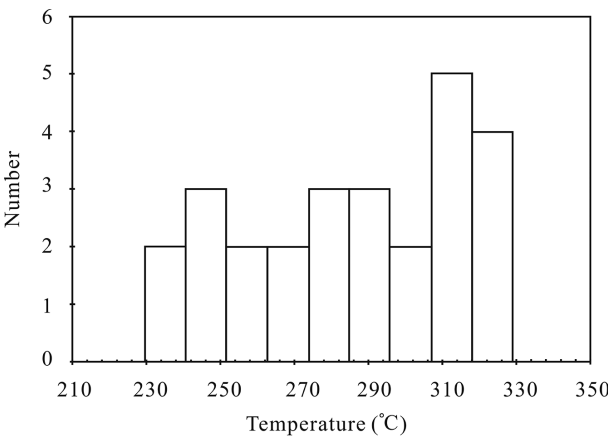

Figure 8. Histogram of homogenization temperatures of fluid inclusions in hydrothermal calcite coexisting with hydrothermal Type 1b zircon from the Tengtie skarn.

Cerium anomalies of in zircon are likely related to the oxidation state of the fluids (Trail et al. 2011), whereas Eu anomalies are more likely related to the REE chemistry of the fluids rather than the redox conditions (Pelleter et al. 2007). Variable Eu anomalies in Type 1b zircons from the Tengtie retrograde skarns indicate that the fluids were spatially compositionally heterogeneous, whereas the generally low-Ce anomalies suggest low-temperature, reducing fluids relative to those precipitating the Type 3 zircons (e.g., Trail et al. 2011). Such a relatively reducing environment is also indicated by the formation of magnetite rather than hematite during the retrograde skarnization (Fig. 2f). The relatively low temperature and reducing affinities of the retrograde heterogeneous fluids might have resulted from the different degrees of mixture between the magmatic and meteoric fluids in different places during retrograde skarnization. Such an interpretation is supported by the oxygen isotopic composition of the Type 1b zircon. The fluid inclusions in calcite, coexisting with the zircon, have homogenization temperatures around of 300 °C (Fig. 8), similar to that reported in slate (Dempster et al. 2004) and high sulfidation deposits (Lawrie et al. 2007). This fluid has a moderate salinity (6.6–17.5 wt% NaCl equiv.). Using this temperature of 300 °C, the oxygen isotopic ratios of the zircon, and corresponding information from Zheng (1993), we calculate $\delta^{18}O$ values of –3.28 to –0.89‰ for the retrograde hydrothermal fluids, which is consistent with the mixing sources involving magmatic and meteoric fluids.

Formation of baddeleyite and zircon during skarnization

Formation of skarns is a dynamic process, involving different hydrothermal stages and a continuous fluid evolution process (Meinert et al. 2005). Our findings in this study clearly provide clues on the mobilization of Zr during skarnization and subsequent formation of baddeleyite and zircon in skarns.

The Mesozoic pluton associated with the Tengtie skarn deposit was derived from the partial melting of Mesoproterozoic continental crust in South China under the tectonic setting of subduction of the paleo-Pacific plate (Gao et al. 2005). The late, fine-grained biotite granite intruded into the Neoproterozoic and Paleozoic strata at 99.3 ± 0.5 Ma (Fig. 5c). In granitic melts, Zr is controlled primarily by zircon, and zircon solubility increases strongly with increasing F (Keppler 1993; Linnen et al. 2014). Incompatible elements, such as Zr and REE, could prefer to concentrate in the fluid-rich residual melt from which the subsolvus granite formed (e.g., Yang et al. 2014). Therefore, in Tengtie, F-rich magmatic-hydrothermal fluids (>650 °C) could have been directly derived from evolved magmas of this granitic phase by magma boiling (Fig. 9a). Such relatively high-temperatures and oxidizing fluids would have contained elevated Zr as $ZrF_n(OH)_m^0$, along with Si, Sn, and some other HSFE. Once the internal hydrostatic pressure became larger than the lithostatic pressure, hydrofracturing was triggered, resulting in the penetration of magmatic-hydrothermal fluids along extensive fractures in the country rocks (e.g., Einaudi et al. 1981; Ciobanu and Cook 2004; Meinert et al. 2005).

At the beginning of skarnization, the Zr-bearing fluids interacted with the surrounding carbonates to produce prograde

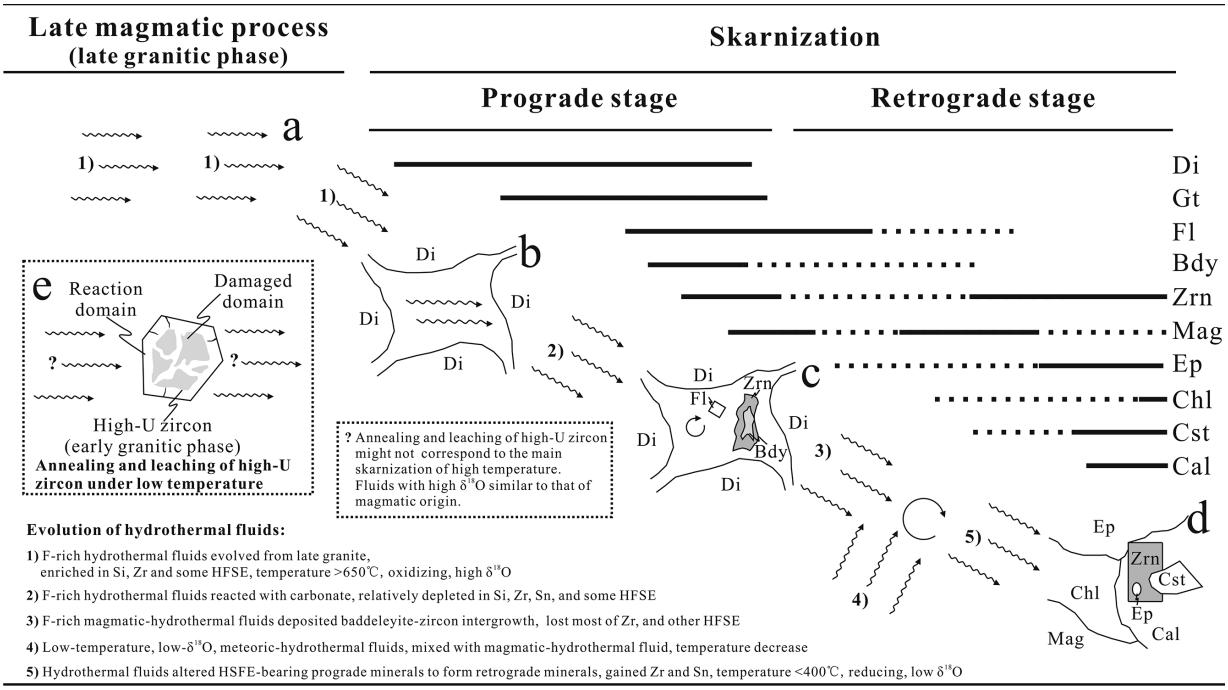

FIGURE 9. Mobilization of Zr and formation process for the baddeleyite and zircon in the Tengtie deposit. The paragenetic sequence of alteration and mineralization in the Tengtie deposit is deduced from the results in this study and data from Zhao and Zhou (2015). (**a**) Fluorine-rich hydrothermal fluids evolved from the late granite. (**b**) Magmatic-hydrothermal fluids interacted with carbonates to form HSFE-bearing prograde skarn minerals, such as diopside. (**c**) Relatively Si-depleted fluids deposited baddeleyite-zircon intergrowth with fluorite in the pores of the prograde skarn minerals. (**d**) Retrograde alteration caused release of Zr and Sn from HSFE-bearing skarn minerals to form zircon and cassiterite with retrograde skarn minerals and magnetite. (**e**) Annealing and leaching of high-U zircon under low temperature. Mineral name abbreviations (Whitney and Evans 2010): baddeleyite = Bdy, calcite = Cal, cassiterite = Cst, chlorite = Chl, diopside = Di, epidote = Ep, fluorite = Fl, garnet = Gt, magnetite = Mag, zircon = Zrn.

skarn minerals (e.g., early diopside), consuming Si with some Zr, Sn, and other HFSE (Fig. 9b), during which porosity in the country rocks was enhanced. Shortly after the deposition of early diopside, Ca activities in the skarn systems were probably still high such that $ZrF_n(OH)^0_m$ broke down to baddeleyite accompanied by fluorite (Fig. 2b) (e.g., Salvi et al. 2000). Notably, the occurrence of baddeleyite in the prograde skarns suggests that during the formation of the early prograde skarn minerals, the fluids were relatively depleted in Si relative to original magmatic-hydrothermal fluids but oversaturated in Zr. Subsequent increase of Si activity, due to continuous input of relatively Si-rich magmatic-hydrothermal fluids, resulted in the decomposition of baddeleyite into the Type 1a zircon rims as observed (Fig. 9c).

Retrograde skarnization was related to the evolved fluids that were depleted in HFSE relative to the prograde fluids. The retrograde skarnization was characterized by alteration of prograde minerals to retrograde minerals (Meinert et al. 2005), during which Zr and Sn with Si in the early prograde skarn minerals (e.g., diopside and garnet), were released into the fluids. The released Zr and Sn were responsible for the formation of cassiterite and Type 1b zircon (97.5 ± 0.7 Ma; Fig. 5a) together with retrograde skarn minerals, such as chlorite, epidote, and calcite (Figs. 2c–2f). Meteoric-hydrothermal fluids must have been involved in the retrograde process, as suggested by the low $\delta^{18}O$ of the hydrothermal Type 1b zircon (–5.1 to –2.7 ‰) (e.g., Cavosie et al. 2005; Kirkland et al. 2009). Finally, hydrothermal Type 1b zircon grains in Tengtie skarns were deposited in a low-temperature (<400 °C), reducing fluid system (Fig. 9d). SIMS dating suggests that the duration of this entire process, from the intrusion of late granitic phase to deposition of retrograde hydrothermal zircon, was less than several million years, which is consistent with the close genetic relationship between the granite and the mineralized skarn, and the short duration of the ore depositional processes normally seen for porphyry systems (e.g., Sillitoe and Mortensen 2010).

IMPLICATIONS

The discovery of abundant hydrothermal zircon and baddeleyite in iron skarns from the Tengtie deposit has important implications for skarnization. Zr was both mobilized and readily deposited as baddeleyite or zircon during different stages of skarnization. Although the fluids for skarnization are commonly assumed to be Si saturated (Meinert et al. 2005), our results show that there was a period of low Si activity relative to original magmatic-hydrothermal fluids due to the formation of pyroxene and garnet during prograde skarnization, which was responsible for the growth of baddeleyite. During the retrograde stage, the growth of zircon was accompanied by mineralization events until a relatively low temperature was reached. This process

may be common in skarns characterized by high-F activities and associated Zr sources.

Determining the absolute duration of magmatic-hydrothermal mineralization events is one of the key questions in geological studies (Meinert et al. 2005; Chiaradia et al. 2013). Ore depositional processes typically span time ranges from tens to a few hundred thousand years constrained by different isotopic dating systems (e.g., Sillitoe and Mortensen 2010; Chelle-Michou et al. 2015). Although it is difficult to assess the uncertainty of different methods (Chiaradia et al. 2013), currently, the precision of U-Pb dating of zircon can be better than 0.1% (e.g., Slama et al. 2008). The results from this study, suggest that the skarnization could occur over several million years. In the future, the precision in dating these processes should improve due to continued development in better instrumentation. Hence, acquisition of reliable ages for hydrothermal zircon and baddeleyite, from both prograde and retrograde skarns, may soon become possible, thus providing a better understanding of the magmatic-hydrothermal mineralization processes.

Acknowledgments

We thank Xiaosong Nie of Chinese Academy of Sciences, and Kencer Ho and Rory Chan of the BMI Technical Consulting (Resources) Limited, Hong Kong, for their assistance in the field. Yazhou Tian of Guizhou University and staffs of associated laboratories are thanked for their help in sample analyses. Special thanks are sent to Paul Robinson of Dalhousie University, Jianfeng Gao of Chinese Academy of Sciences, Kwan-Nan Pang of Academia Sinica, Chris McFariane of University of New Brunswick, Don Davis of University of Toronto, and Xuran Zuo of The University of Hong Kong, for their constructive suggestions and support. Also, we sincerely thank Daniel Harlov and two anonymous reviewers for providing very thorough suggestions. This research was financially supported by HKU CRCG Small Project Funding (201309176142) and Thousand Youth Talents Plan grant to Wei Terry Chen.

References cited

Ague, J.J. (1994) Mass transfer during Barrovian metamorphism of pelites, south-central Connecticut. I: Evidence for changes in composition and volume. American Journal of Science, 294, 989–1057.

——— (2003) Fluid infiltration and transport of major, minor, and trace elements during regional metamorphism of carbonate rocks, Wepawaug Schist, Connecticut, USA. American Journal of Science, 303, 753–816.

——— (2011) Extreme channelization of fluid and the problem of element mobility during Barrovian metamorphism. American Mineralogist, 96, 333–352.

Bebout, G.E., Ryan, J.G., Leeman, W.P., and Bebout, A.E. (1999) Fractionation of trace elements by subduction-zone metamorphism—effect of convergent-margin thermal evolution. Earth and Planetary Science Letters, 171, 63–81.

Bodnar, R.J. (1994) Synthetic fluid inclusions: XII. The system H_2O-NaCl. Experimental determination of the halite liquidus and isochores for a 40 wt% NaCl solution. Geochimica et Cosmochimica Acta, 58, 1053–1063.

Breeding, C.M., Ague, J.J., and Bröcker, M. (2004) Fluid–metasedimentary rock interactions in subduction-zone mélange: Implications for the chemical composition of arc magmas. Geology, 32, 1041–1044.

Cavosie, A.J., Valley, J.W., and Wilde, S.A. (2005) Magmatic $\delta^{18}O$ in 4400–3900 Ma detrital zircons: A record of the alteration and recycling of crust in the Early Archean. Earth and Planetary Science Letters, 235, 663–681.

Chelle-Michou, C., Chiaradia, M., Selby, D., Ovtcharova, M., and Spikings, R.A. (2015) High-resolution geochronology of the Coroccohuayco porphyry-skarn deposit, Peru: A rapid product of the Incaic Orogeny. Economic Geology, 110, 423–443.

Chen, J.F., and Jahn, B.M. (1998) Crustal evolution of southeastern China: Nd and Sr isotopic evidence. Tectonophysics, 284, 101–133.

Chen, D.Z., Tucker, M.E., Jiang, M.S., and Zhu, J.Q. (2001) Long-distance correlation between tectonic-controlled, isolated carbonate platforms by cyclostratigraphy and sequence stratigraphy in the Devonian of South China. Sedimentology, 48, 57–78.

Cheng, S.B., Fu, J.M., Xu, D.M., Chen, X.Q., Ma, L.-Y., Wang, X.D., and Pang, Y.C. (2009) Zircon SHRIMP U-Pb dating and geochemical characteristics of Daning batholith in northeast Guangxi. Geology in China, 36, 1278–1288.

Chiaradia, M., Schaltegger, U., Spikings, R., Wotzlaw, J.F., and Ovtcharova, M. (2013) How accurately can we date the duration of magmatic-hydrothermal events in porphyry systems?—An invited paper. Economic Geology, 108, 565–584.

Ciobanu, C.L., and Cook, N.J. (2004) Skarn textures and a case study: the Ocna de Fier-Dognecea orefield, Banat, Romania. Ore Geology Reviews, 24, 315–370.

Davidson, A., and Van Breemen, O. (1988) Baddeleyite-zircon relationships in coronitic metagabbro, Grenville Province, Ontario: implications for geochronology. Contributions to Mineralogy and Petrology, 100, 291–299.

Dempster, T.J., Hay, D.C., and Bluck, B.J. (2004) Zircon growth in slate. Geology, 32, 221–224.

Deng, X.-D., Li, J.-W., and Wen, G. (2015) U-Pb geochronology of hydrothermal zircons from the early Cretaceous iron skarn deposits in the Handan-Xingtai district, North China craton. Economic Geology, 110, 2159–2180.

Drummond, M.S., Defant, M.J., and Kepezhinskas, P.K. (1996) Petrogenesis of slab-derived trondhjemite-tonalite-dacite/adakite magmas. Geological Society of America Special Papers, 315, 205–215.

Einaudi, M.T., Meinert, L.D., and Newberry, R.J. (1981) Skarn deposits. Economic Geology, 75, 317–391.

Ernst, R.E., and Buchan, K.L. (2003) Recognizing mantle plumes in the geological record. Annual Review of Earth and Planetary Sciences, 31, 469–523.

Floyd, P.A., and Winchester, J.A. (1975) Magma type and tectonic setting discrimination using immobile elements. Earth and Planetary Science Letters, 27, 211–218.

Gao, J.F., Ling, H.F., Sheng, W.Z., Lu, J.J., Zhang, M., Huang, G.L., and Tan, Z.Z. (2005) Geochemistry and petrogenesis of Lianyang granite composite, west Guangdong province. Acta Petrologica Sinica, 21, 1645–1656.

Gaspar, M., Knaack, C., Meinert, L.D., and Moretti, R. (2008) REE in skarn systems: A LA-ICP-MS study of garnets from the Crown Jewel gold deposit. Geochimica et Cosmochimica Acta, 72, 185–205.

Geisler, T., Ulonska, M., Schleicher, H., Pidgeon, R.T., and van Bronswijk, W. (2001) Leaching and differential recrystallization of metamict zircon under experimental hydrothermal conditions. Contributions to Mineralogy and Petrology, 141, 53–65.

Geisler, T., Rashwan, A.A., Rahn, M.K.W., Poller, U., Zwingmann, H., Pidgeon, R.T., Schleicher, H., and Tomaschek, F. (2003) Low-temperature hydrothermal alteration of natural metamict zircons from the Eastern Desert, Egypt. Mineralogical Magazine, 67, 485–508.

Geisler, T., Schaltegger, U., and Tomaschek, F. (2007) Re-equilibration of zircon in aqueous fluids and melts. Elements, 3, 43–50.

Gieré, R. (1986) Zirconolite, allanite and hoegbomite in a marble skarn from the Bergell contact aureole—Implications for mobility of Ti, Zr and REE. Contributions to Mineralogy and Petrology, 93, 459–470.

Gieré, R., and Williams, C.T. (1992) REE-bearing minerals in a Ti-rich vein from the Adamello contact aureole (Italy). Contributions to Mineralogy and Petrology, 112, 83–100.

Haas, J.R., Shock, E.L., and Sassani, D.C. (1995) Rare earth elements in hydrothermal systems: estimates of standard partial molal thermodynamic properties of aqueous complexes of the rare earth elements at high pressures and temperatures. Geochimica et Cosmochimica Acta, 59, 4329–4350.

He, Z., Huang, F., Yu, H., Xiao, Y., Wang, F., Li, Q., Xia, Y., and Zhang, X. (2015) A flux-free fusion technique for rapid determination of major and trace elements in silicate rocks by LA-ICP-MS. Geostandards and Geoanalytical Research, 40, 5–27.

Hoskin, P.W.O. (2005) Trace-element composition of hydrothermal zircon and the alteration of Hadean zircon from the Jack Hills, Australia. Geochimica et Cosmochimica Acta, 69, 637–648.

Hu, R.Z., and Zhou, M.F. (2012) Multiple Mesozoic mineralization events in South China—an introduction to the thematic issue. Mineralium Deposita, 47, 579–588.

Ismail, R., Ciobanu, C.L., Cook, N.J., Teale, G.S., Giles, D., Mumm, A.S., and Wade, B. (2014) Rare earths and other trace elements in minerals from skarn assemblages, Hillside iron oxide-copper-gold deposit, Yorke Peninsula, South Australia. Lithos, 184, 456–477.

Keppler, H. (1993) Influence of fluorine on the enrichment of high field strength trace elements in granitic rocks. Contributions to Mineralogy and Petrology, 114, 479–488.

Kerrich, R., and King, R. (1993) Hydrothermal zircon and baddeleyite in Val-Dor Archean mesothermal gold deposits—Characteristics, compositions, and fluid-inclusion properties, with implications for timing of primary gold mineralization. Canadian Journal of Earth Sciences, 30, 2334–2351.

Kirkland, C.L., Whitehouse, M.J., and Slagstad, T. (2009) Fluid-assisted zircon and monazite growth within a shear zone: a case study from Finnmark, Arctic Norway. Contributions to Mineralogy and Petrology, 158, 637–657.

Kusiak, M.A., Dunkley, D.J., Słaby, E., Martin, H., and Budzyń, B. (2009) Sensitive high-resolution ion microprobe analysis of zircon reequilibrated by late magmatic fluids in a hybridized pluton. Geology, 37, 1063–1066.

Lawrie, K.C., Mernagh, T.P., Ryan, C.G., van Achterbergh, E., and Black, L.P. (2007) Chemical fingerprinting of hydrothermal zircons: An example from the Gidginbung high sulphidation Au-Ag-(Cu) deposit, New South Wales, Australia. Proceedings of the Geologists Association, 118, 37–46.

Li, X.H., Liu, Y., Li, Q.L., Guo, C.H., and Chamberlain, K.R. (2009) Precise determination of Phanerozoic zircon Pb/Pb age by multicollector SIMS without external standardization. Geochemistry, Geophysics, Geosystems, 10, 1525–2027.

Li, X.H., Long, W.G., Li, Q.L., Liu, Y., Zheng, Y.F., Yang, Y.H., Chamberlain, K.R., Wan, D.F., Guo, C.H., and Wang, X.C. (2010) Penglai zircon megacrysts: a potential new working reference material for microbeam determination of Hf-O isotopes and U-Pb age. Geostandards and Geoanalytical Research, 34, 117–134.

Linnen, R.L., Samson, I.M., Williams-Jones, A.E., and Chakhmouradian, A.R. (2014). Geochemistry of the rare-earth element, Nb, Ta, Hf, and Zr deposits. In H.D.H.K. Turekian, Ed., Treatise on Geochemistry (2nd ed.), p. 543–568. Elsevier.

Liu, Y.S., Gao, S., Hu, Z.C., Gao, C.G., Zong, K.Q., and Wang, D.B. (2010) Continental and oceanic crust recycling-induced melt-peridotite interactions in the Trans-North China Orogen: U-Pb dating, Hf isotopes and trace elements in zircons from mantle xenoliths. Journal of Petrology, 51, 537–571.

Mao, J.W., Cheng, Y.B., Chen, M.H., and Pirajno, F. (2013) Major types and time-space distribution of Mesozoic ore deposits in South China and their geodynamic settings. Mineralium Deposita, 48, 267–294.

McDonough, W.F., and Sun, S.S. (1995) The composition of the Earth. Chemical Geology, 120, 223–253.

McLaren, A.C., Gerald, J.D.F., and Williams, I.S. (1994) The microstructure of zircon and its influence on the age determination from Pb/U isotopic ratios measured by ion microprobe. Geochimica et Cosmochimica Acta, 58, 993–1005.

Meinert, L., Dipple, G., and Nicolescu, S. (2005) World skarn deposits. Economic Geology, 100, 299–336.

Mezger, K., and Krogstad, E.J. (1997) Interpretation of discordant U-Pb zircon ages: An evaluation. Journal of Metamorphic Geology, 15, 127–140.

Migdisov, A.A., and Williams-Jones, A.E. (2007) An experimental study of the solubility and speciation of neodymium (III) fluoride in F-bearing aqueous solutions. Geochimica et Cosmochimica Acta, 71, 3056–3069.

Migdisov, A.A., Williams-Jones, A.E., and Wagner, T. (2009) An experimental study of the solubility and speciation of the Rare Earth Elements (III) in fluoride-and chloride-bearing aqueous solutions at temperatures up to 300 °C. Geochimica et Cosmochimica Acta, 73, 7087–7109.

Migdisov, A.A., Williams-Jones, A.E., van Hinsberg, V., and Salvi, S. (2011) An experimental study of the solubility of baddeleyite (ZrO_2) in fluoride-bearing solutions at elevated temperature. Geochimica et Cosmochimica Acta, 75, 7426–7434.

Moine, B., Ramambazafy, A., Rakotondrazafy, M., Ravololomiandrinarivo, B., Cuney, M., and De Parseval, P. (1998) The role of fluor-rich fluids in the formation of the thorianite and sapphire deposits from SE Madagascar. Mineralogical Magazine, 62, 999–1000.

Mursic, Z., Vogt, T., Boysen, H., and Frey, F. (1992) Single-crystal neutron diffraction study of metamict zircon up to 2000 K. Journal of Applied Crystallography, 25, 519–523.

Nasdala, L., Beran, A., Libowitzky, E., and Wolf, D. (2001) The incorporation of hydroxyl groups and molecular water in natural zircon ($ZrSiO_4$). American Journal of Science, 301, 831–857.

Nesbitt, R.W., Pascual, E., Fanning, C.M., Toscano, M., Saez, R., and Almodovar, G.R. (1999) U-Pb dating of stockwork zircons from the eastern Iberian Pyrite Belt. Journal of the Geological Society, 156, 7–10.

Pearce, J.A. (1996) Sources and settings of granitic rocks. Episodes, 19, 120–125.

——— (2008) Geochemical fingerprinting of oceanic basalts with applications to ophiolite classification and the search for Archean oceanic crust. Lithos, 100, 14–48.

Pearce, J.A., and Cann, J.R. (1973) Tectonic setting of basic volcanic rocks determined using trace element analyses. Earth and Planetary Science Letters, 19, 290–300.

Pelleter, E., Cheilletz, A., Gasquet, D., Mouttaqi, A., Annich, M., El Hakour, A., Deloule, E., and Feraud, G. (2007) Hydrothermal zircons: A tool for ion microprobe U-Pb dating of gold mineralization (Tamlalt-Menhouhou gold deposit Morocco). Chemical Geology, 245, 135–161.

Penniston-Dorland, S.C., and Ferry, J.M. (2008) Element mobility and scale of mass transport in the formation of quartz veins during regional metamorphism of the Waits River Formation, east-central Vermont. American Mineralogist, 93, 7–21.

Pettke, T., Audetat, A., Schaltegger, U., and Heinrich, C.A. (2005) Magmatic-to-hydrothermal crystallization in the W-Sn mineralized Mole Granite (NSW, Australia)—Part II: Evolving zircon and thorite trace element chemistry. Chemical Geology, 220, 191–213.

Pidgeon, R.T., Nemchin, A.A., and Cliff, J. (2013) Interaction of weathering solutions with oxygen and U-Pb isotopic systems of radiation-damaged zircon from an Archean granite, Darling Range Batholith, Western Australia. Contributions to Mineralogy and Petrology, 166, 511–523.

Rizvanova, N.G., Levchenkov, O.A., Belous, A.E., Bezmen, N.I., Maslenikov, A.V., Komarov, A.N., Makeev, A.F., and Levskiy, L.K. (2000) Zircon reaction and stability of the U-Pb isotope system during interaction with carbonate fluid: experimental hydrothermal study. Contributions to Mineralogy and Petrology, 139, 101–114.

Rubenach, M. (2013). Structural controls of metasomatism on a regional scale. In D.E. Harlov and A. Håkon, Eds., Metasomatism and the Chemical Transformation of Rock, p. 93–140. Springer.

Rubin, J.N., Henry, C.D., and Price, J.G. (1989) Hydrothermal zircons and zircon overgrowths, Sierra-Blanca Peaks, Texas. American Mineralogist, 74, 865–869.

——— (1993) The mobility of zirconium and other immobile elements during hydrothermal alteration. Chemical Geology, 110, 29–47.

Salvi, S., and Williams-Jones, A.E. (1996) The role of hydrothermal processes in concentrating high-field strength elements in the Strange Lake peralkaline complex, northeastern Canada. Geochimica et Cosmochimica Acta, 60, 1917–1932.

Salvi, S., Fontan, F., Monchoux, P., Williams-Jones, A., and Moine, B. (2000) Hydrothermal mobilization of high field strength elements in alkaline igneous systems: evidence from the Tamazeght Complex (Morocco). Economic Geology, 95, 559–576.

Sillitoe, R.H., and Mortensen, J.K. (2010) Longevity of porphyry copper formation at Quellaveco, Peru. Economic Geology, 105, 1157–1162.

Slama, J., Kosler, J., Condon, D.J., Crowley, J.L., Gerdes, A., Hanchar, J.M., Horstwood, M.S.A., Morris, G.A., Nasdala, L., Norberg, N., and others (2008) Plesovice zircon—A new natural reference material for U-Pb and Hf isotopic microanalysis. Chemical Geology, 249, 1–35.

Smith, M.P., Henderson, P., Jeffries, T.E.R., Long, J., and Williams, C.T. (2004) The rare earth elements and uranium in garnets from the Beinn an Dubhaich Aureole, Skye, Scotland, UK: constraints on processes in a dynamic hydrothermal system. Journal of Petrology, 45, 457–484.

Söderlund, U., Hellström, F.A., and Kamo, S.L. (2008) Geochronology of high-pressure mafic granulite dykes in SW Sweden: tracking the P-T-t path of metamorphism using Hf isotopes in zircon and baddeleyite. Journal of Metamorphic Geology, 26, 539–560.

Solar, G.S., and Brown, M. (2001) Petrogenesis of migmatites in Maine, USA: possible source of peraluminous leucogranite in plutons? Journal of Petrology, 42, 789–823.

Tang, G.-Q., Li, X.-H., Li, Q.-L., Liu, Y., Ling, X.-X., and Yin, Q.-Z. (2015) Deciphering the physical mechanism of the topography effect for oxygen isotope measurements using a Cameca IMS-1280 SIMS. Journal of Analytical Atomic Spectrometry, 30, 950–956.

Toscano, M., Pascual, E., Nesbitt, R., Almodóvar, G., Sáez, R., and Donaire, T. (2014) Geochemical discrimination of hydrothermal and igneous zircon in the Iberian Pyrite Belt, Spain. Ore Geology Reviews, 56, 301–311.

Trail, D., Watson, E.B., and Tailby, N.D. (2011) The oxidation state of Hadean magmas and implications for early Earth's atmosphere. Nature, 480, 79–82.

Tropper, P., Manning, C.E., and Harlov, D.E. (2011) Solubility of $CePO_4$ monazite and YPO_4 xenotime in H_2O and H_2O-NaCl at 800 °C and 1GPa: implications for REE and Y transport during high-grade metamorphism. Chemical Geology, 282, 58–66.

——— (2013) Experimental determination of $CePO_4$ and YPO_4 solubilities in H_2O-NaF at 800 °C and 1GPa: implications for rare earth element transport in high-grade metamorphic fluids. Geofluids, 13, 372–380.

Valley, J.W. (2003) Oxygen isotopes in zircon. Reviews in Mineralogy and Geochemistry, 53, 343–386.

Wang, X.-L., Coble, M.A., Valley, J.W., Shu, X.-J., Kitajima, K., Spicuzza, M.J., and Sun, T. (2014) Influence of radiation damage on Late Jurassic zircon from southern China: Evidence from in situ measurements of oxygen isotopes, laser Raman, U–Pb ages, and trace elements. Chemical Geology, 389, 122–136.

White, L.T., and Ireland, T.R. (2012) High-uranium matrix effect in zircon and its implications for SHRIMP U-Pb age determinations. Chemical Geology, 306, 78–91.

Whitney, D.L., and Evans, B.W. (2010) Abbreviations for names of rock-forming minerals. American Mineralogist, 95, 185–187.

Williams-Jones, A.E., and Migdisov, A.A. (2014) Experimental constraints on the transport and deposition of metals in ore-forming hydrothermal systems. Society of Economic Geologists, 18, 77–96.

Williams-Jones, A.E., Migdisov, A.A., and Samson, I.M. (2012) Hydrothermal mobilisation of the rare earth elements—a tale of "ceria" and "yttria". Elements, 8, 355–360.

Yan, D.P., Zhou, M.F., Song, H.L., Wang, X.W., and Malpas, J. (2003) Origin and tectonic significance of a Mesozoic multi-layer over-thrust system within the Yangtze Block (South China). Tectonophysics, 361, 239–254.

Yang, W.-B., Niu, H.-C., Shan, Q., Sun, W.-D., Zhang, H., Li, N.-B., Jiang, Y.-H., and Yu, X.-Y. (2014) Geochemistry of magmatic and hydrothermal zircon from the highly evolved Baerzhe alkaline granite: implications for Zr-REE-Nb mineralization. Mineralium Deposita, 49, 451–470.

Yu, J.H., Zhou, X.M., O'Reilly, Y.S., Zhao, L., Griffin, W.L., Wang, R.C., Wang, L.J., and Chen, X.M. (2005) Formation history and protolith characteristics of granulite facies metamorphic rock in Central Cathaysia deduced from U-Pb and Lu-Hf isotopic studies of single zircon grains. Chinese Science Bulletin, 50, 2080–2089.

Zhao, W.W., and Zhou, M.-F. (2015) In-situ LA–ICP-MS trace elemental analyses of magnetite: The Mesozoic Tengtie skarn Fe deposit in the Nanling Range, South China. Ore Geology Reviews, 65, 872–883.

Zhao, J.H., Zhou, M.F., Yan, D.P., Zheng, J.P., and Li, J.W. (2011) Reappraisal of the ages of Neoproterozoic strata in South China: No connection with the Grenvillian orogeny. Geology, 39, 299–302.

Zheng, Y.-F. (1993) Calculation of oxygen isotope fractionation in anhydrous silicate minerals. Geochimica et Cosmochimica Acta, 57, 1079–1079.

Zhou, M.F., Yan, D.P., Kennedy, A.K., Li, Y.Q., and Ding, J. (2002) SHRIMP U-Pb zircon geochronological and geochemical evidence for Neoproterozoic arc-magmatism along the western margin of the Yangtze Block, South China. Earth and Planetary Science Letters, 196, 51–67.

Zhou, X.M., Sun, T., Shen, W.Z., Shu, L.S., and Niu, Y.L. (2006) Petrogenesis of Mesozoic granitoids and volcanic rocks in South China: A response to tectonic evolution. Episodes, 29, 26–33.

Manuscript received February 1, 2016
Manuscript accepted July 6, 2016
Manuscript handled by Daniel Harlov